HHS Public Access

Author manuscript

Phys Med Biol. Author manuscript; available in PMC 2018 January 21.

Published in final edited form as:

Phys Med Biol. 2017 January 21; 62(2): 484–500. doi:10.1088/1361-6560/aa4f6f.

Attenuation Measuring Ultrasound Shearwave Elastography and *in vivo* application in post-transplant liver patients

Ivan Z. Nenadic[1], **Bo Qiang**[1], **Matthew W. Urban**[1,2], **Heng Zhao**[4], **William Sanchez**[3], **James F. Greenleaf**[1], and **Shigao Chen**[1,2]

[1]Department of Physiology and Biomedical Engineering, Mayo Clinic College of Medicine, Rochester, MN, USA

[2]Department of Radiology, Mayo Clinic College of Medicine, Rochester, MN, USA

[3]Department of Medicine, Division of Gastroenterology and Hepatology, Mayo Clinic College of Medicine, Rochester, MN, USA

[4]Sonavation Inc., Palm Beach Gardens, FL, USA

Abstract

Ultrasound and magnetic resonance elastography techniques are used to assess mechanical properties of soft tissues. Tissue stiffness is related to various pathologies such as fibrosis, loss of compliance, and cancer. One way to perform elastography is measuring shear wave velocity of propagating waves in tissue induced by intrinsic motion or an external source of vibration, and relating the shear wave velocity to tissue elasticity. All tissues are inherently viscoelastic and ignoring viscosity biases the velocity-based estimates of elasticity and ignores a potentially important parameter of tissue health. We present Attenuation Measuring Ultrasound Shearwave Elastography (AMUSE), a technique that independently measures both shear wave velocity and attenuation in tissue and therefore allows characterization of viscoelasticity without using a rheological model. The theoretical basis for AMUSE is first derived and validated in finite element simulations. AMUSE is validated against the traditional methods for assessing shear wave velocity (phase gradient) and attenuation (amplitude decay) in tissue mimicking phantoms and excised tissue. The results agreed within one standard deviation. AMUSE was used to measure shear wave velocity and attenuation in 15 transplanted livers in patients with potential acute rejection, and the results were compared with the biopsy findings in a preliminary study. The comparison showed excellent agreement and suggests that AMUSE can be used to separate transplanted livers with acute rejection from livers with no rejection.

Introduction

Palpation is an important part of a medical exam during which mechanical properties of a tissue are evaluated by manual compression in an effort to assess changes in tissue elasticity and viscosity. Elastic and viscous properties of a material can be obtained by inducing a monochromatic wave into the region of interest and measuring the velocity and attenuation (rate of amplitude decay) of the propagated wave.

Over the past several decades, the fields of ultrasound and magnetic resonance (MR) elastography have developed various techniques to measure mechanical properties of tissues (Sarvazyan *et al.*, 2011; Tanter and Fink, 2014). The basic principle of these techniques is the use of an external vibrator or focused ultrasound to create waves in the tissue, and application of ultrasound or magnetic resonance imaging (MRI) to measure the wave propagation as a function of time and distance. Various algorithms are then used to calculate the velocity of the propagated shear wave (Chen *et al.*, 2009; Bercoff *et al.*, 2004). Using these measurements much effort has been paid to characterizing soft tissues with models of varying degree. Assuming that the tissue is linear, homogeneous, isotropic, and purely elastic, the wave velocity (c) is directly related to the elastic modulus (μ) of the tissue via $\mu = \rho c^2$, where ρ is the tissue mass density (close to that of water). These elasticity measurement techniques have been applied to demonstrate changes in wave velocity in the myocardium and arteries throughout the heart cycle in animals *in vivo*, increased wave velocity in liver fibrosis and cirrhosis, breast and thyroid cancer, and anisotropic wave velocities relative to the muscle fiber orientation (Nenadic *et al.*, 2011; Couade *et al.*, 2010; Couade *et al.*, 2011; Bernal *et al.*, 2011; Chen *et al.*, 2009; Gennisson *et al.*, 2010; Sarvazyan *et al.*, 2011; Tanter *et al.*, 2008; Sebag *et al.*, 2010).

However, all biological tissues are inherently viscoelastic and most elastography techniques assume the tissues are solely elastic and thus ignore the viscosity. Ignoring the viscous component not only biases the velocity-derived estimates of elasticity but also fails to report a potentially important tissue parameter. In addition, disregarding tissue viscosity masks potentially complex pathophysiological changes that manifest in structural changes affecting both elasticity and viscosity by grouping the two terms under the elasticity parameter. Multiple reports of animal and human studies characterizing liver viscoelasticity using magnetic resonance elastography (MRE) have been reported (Asbach *et al.*, 2008; Asbach *et al.*, 2010; Klatt *et al.*, 2010; Leclerc *et al.*, 2013; Sinkus *et al.*, 2005). Among the ultrasound-based methods are supersonic shear imaging (SSI) (Muller *et al.*, 2009) and shearwave dispersion ultrasound vibrometry (SDUV) (Chen *et al.*, 2013). Analysis of phase velocity dispersion has been used for liver fibrosis staging and for analyzing how steatosis affects viscoelasticity (Nightingale *et al.*, 2015).

The omission of tissue viscosity largely stems from the inability to make stable and reproducible measurements of shear wave attenuation. Tissue shear wave attenuation is a measure of how fast the shear wave energy dissipates in the tissue. Several techniques have used model-based methods that estimate tissue viscosity by measuring wave velocity at multiple frequencies (wave velocity dispersion) and fit a dual- or multi-parameter rheological model to the wave velocity dispersion to estimate tissue elasticity and viscosity (Deffieux *et al.*, 2009; Chen *et al.*, 2009). A significant issue with these models (besides being models that may not describe the true viscoelastic relationships) is that they assume a fixed relationship between wave velocity and attenuation strictly based on the velocity measurements and without any knowledge of tissue attenuation at different frequencies. Because of the difficulty to measure tissue attenuation *in vivo*, these models cannot be verified. Thus, rheological model-free measurement of tissue viscoelasticity requires measurements of wave velocity and attenuation at a given frequency. Here, we present such

a method and refer to it as Attenuation Measuring Ultrasound Shearwave Elastography, or AMUSE. It should be noted that this method assumes a linear, homogeneous, isotropic, and viscoelastic medium, but no particular rheological model. AMUSE is a new method developed by our group that measures shear wave velocity and attenuation without a rheological model for characterization of tissue mechanical properties.

In its basic implementation, AMUSE requires the presence of a mechanical wave propagating in tissue and the ability to track tissue motion in the spatiotemporal domain. As both MR and ultrasound elastography techniques measure shear wave propagation in tissue, AMUSE could be applied across different shear wave elasticity techniques. A two-dimensional Fourier Transform (2D FT) of the tissue motion as a function of time (t) and distance (x) results in the frequency (f) versus wave number (k) domain, also known as the k-space. The shear wave velocity and attenuation are directly related to the location and shape of the k-space magnitude maxima. The relationship between the shape of the peak in the k-space and the wave attenuation was derived and validated by our group and has not been reported before. The AMUSE shear wave velocity and attenuation is compared to the values obtained using laboratory reference method (gold standard) to estimate shear wave velocity through the phase gradient and the shear wave attenuation through the amplitude decay. Comparative studies in finite element models, a polyvinyl alcohol (PVA) phantom and an excised pig liver were performed evaluate the agreement between AMUSE and the laboratory reference methods. AMUSE was used to measure mechanical properties of post-transplant livers with the potential of acute cellular rejection in patients and the results were correlated with biopsy findings.

Methods

Theory

Consider a source-free, one-dimensional, plane, harmonic, shear wave propagating in a linear, homogeneous, isotropic, viscoelastic medium that is described by the following equation,

$$\frac{\partial^2 u}{\partial t^2} - \frac{G^*}{\rho}\frac{\partial^2 u}{\partial x^2} = 0 \quad \text{(Eq. 1)}$$

where u is the displacement, x and t are the spatial and time variables and always positive, respectively. G^* is the complex shear modulus and ρ is the mass density. The fundamental equations of shear wave propagation can be found in (Achenbach, 2005; Graff, 1975; Kundu, 2003). The steady-state solution to Eq. for the case of a monochromatic wave is shown in Eq. (2):

$$u(x,t) = u_0 e^{i\omega_0 t} e^{ik_0 x} \quad \text{(Eq. 1)}$$

where $\omega_0 = 2\pi f_0$ is the angular frequency, f_0 is the frequency of the wave, and u_0 is the amplitude (at $x = 0$, $t = 0$) of the wave and is a real number. The complex wave number k_0 can be expressed in terms of angular frequency ω_0, wave speed c and attenuation $\alpha(> 0)$ as,

$$k_0 = \frac{\omega_0}{c} + i\alpha \quad \text{(Eq. 2)}$$

Combining Eq. (1) and Eq. (2) gives,

$$u(x,t) = u_0 e^{i\omega_0 t} e^{i\left(\frac{\omega_0}{c}\right)x} e^{-\alpha x} = u_0 \left[e^{-\alpha x} e^{i\omega_0 \frac{x}{c}}\right] \left[e^{i\omega_0 t}\right], \quad \text{(Eq. 3)}$$

Transforming $u(x, t)$ to what we have termed "k-space" by taking 2D Fourier transform,

$$U(k,f) = \int_{-\infty}^{\infty}\int_{-\infty}^{\infty} u(x,t) e^{-i2\pi(kx+ft)} dx dt \quad \text{(Eq. 4)}$$

where k and f are the wave number and frequency variables, respectively. Both of these variables are real. Because the two parts with x and t in Eq. (3) are separable, Eq. (4) can be simplified to,

$$U(k,f) = u_0 \times FT_t\{e^{i\omega_0 t}\} \times FT_x\left\{e^{-\alpha x} e^{i\omega_0 \frac{x}{c}}\right\} \quad \text{(Eq. 5)}$$

where $FT_t\{.\}FT_t\{\cdot\}$ and $FT_x\{.\}$ $FT_x\{\cdot\}$ are one-dimensional (1D) Fourier transforms applied to the time and spatial domains, respectively. They are defined as,

$$FT_t\{g(t)\} = \int_{-\infty}^{\infty} g(t) e^{-i2\pi ft} dt \quad \text{(Eq. 6)}$$

$$FT_x\{h(x)\} = \int_{-\infty}^{\infty} h(x) e^{-i2\pi kx} dx \quad \text{(Eq. 7)}$$

Note that,

$$FT_t\{e^{i\omega_0 t}\} = FT_t\{e^{i2\pi f_0 t}\} = \delta(f - f_0), \quad \text{(Eq. 8)}$$

$$FT_x\left\{e^{-\alpha x}e^{i\omega_0\frac{x}{c}}\right\}=\frac{1}{\alpha+i2\pi k}\otimes\delta\left(k-\frac{f_0}{c}\right)=\frac{1}{\alpha+i2\pi\left(k-\frac{f_0}{c}\right)} \quad \text{(Eq. 9)}$$

where $\delta(\cdot)$ is the Dirac delta function and $\otimes$ is the convolution operation. Substituting the corresponding parts in Eq. (5) with Eq. (8) and Eq. (9) gives,

$$U(k,f)=\frac{u_0\delta(f-f_0)}{\alpha+i2\pi\left(k-\frac{f_0}{c}\right)} \quad \text{(Eq. 10)}$$

Its magnitude can be expressed as,

$$|U(k,f)|=\frac{u_0\delta(f-f_0)}{\sqrt{\alpha^2+4\pi^2\left(k-\frac{f_0}{c}\right)^2}} \quad \text{(Eq. 11)}$$

Equation (11) shows that for a wave with frequency f_0, the magnitude of its transform in k-space has a corresponding peak at $(k, f) = (f_0/c, f_0)$. Shear wave velocity (c) can be calculated by dividing the frequency (f_0) and wave number (k_{max}) coordinates of the peak so that $c = f_0/k_{max}$.

Now, let us consider the derivation of the wave attenuation from k-space. In practice, the amplitude at f_0 is not infinite as the delta function would imply, but has finite amplitude. Denoting this function as $\hat{\delta}(0)$ and defining $u_0\hat{\delta}(0) \equiv 2A$, for reasons that will shortly be explained we obtain

$$|U(k,f)|_{f=f_0}=|U(k,f_0)|=\frac{2A}{\sqrt{\alpha^2+4\pi^2\left(k-\frac{f_0}{c}\right)^2}} \quad \text{(Eq. 12)}$$

The maximum amplitude of Eq. (13) is,

$$|U(k,f_0)|_{max}=\left|U\left(\frac{f_0}{c},f_0\right)\right|=\frac{2A}{\alpha} \quad \text{(Eq. 13)}$$

At half-maximum magnitude,

$$\frac{2A}{\sqrt{\alpha^2+4\pi^2\left(k-\frac{f_0}{c}\right)^2}}=\frac{|U(k,f_0)|_{max}}{2}=\frac{A}{\alpha} \quad \text{(Eq. 14)}$$

Solving for k, the two solutions are,

$$k_{1,2}=\pm\frac{\sqrt{3}}{2\pi}\alpha+\frac{f_0}{c} \quad \text{(Eq. 15)}$$

Therefore, the full-width at half-maximum (*FWHM*) is,

$$FWHM=|k_1-k_2|=\frac{\sqrt{3}}{\pi}\alpha \quad \text{(Eq. 16)}$$

Using this result, wave attenuation at a particular frequency can then be estimated as,

$$\alpha=\frac{FWHM\times\pi}{\sqrt{3}} \quad \text{(Eq. 17)}$$

For some ultrasound elastography methods, the particle velocity instead of displacement is the raw measurement. The particle velocity is the time derivative of the displacement, so the differentiation property of the Fourier transform can be applied. It can be proven that Eq. (18) still holds in this case.

Eqs. (16)–(18) could be avoided by observing that the left-hand side of Eq. (15) is a Lorentzian distribution centered at f_0/c and the *FWHM* property follows by definition.

After attenuation is estimated, the complex wave number k_0 can be calculated using Eq. (3) and the material complex shear modulus can be estimated as,

$$G=G_S+iG_L=\rho\left(\frac{\omega_0}{k_0}\right)^2=\rho\left(\frac{\omega_0}{\frac{\omega_0}{c}+i\alpha}\right)^2 \quad \text{(Eq. 18)}$$

where G_S and G_L are the storage and loss shear moduli.

Thus, both the shear wave velocity and attenuation can be calculated from the 2D FT of the tissue displacement as a function of time and distance, and the complex shear wave number can be recovered without a rheological model in the medium assumed in Eq. (1).

The impulsive focused acoustic radiation force produces a cylindrical wave whose energy dissipates via cylindrically shaped wave fronts of increasing radius as the wave propagates away from the source. The cylindrical wave front is different than the plane wave front, and the equation of particle motion in the direction of wave propagation (x) is governed by

$$u_z(x,t)=\frac{i}{4}H_0^{(1)}(k_0^* x)e^{i\omega_0 t} \quad \text{(Eq. 20)}$$

where $H_0^{(1)}$ is the zeroth-order Hankel function, and $k_0=\frac{\omega_0}{c}+i\alpha$ is the complex wave number. In the limit of $(k_0 x) \gg 0$, equation (20) converges to:

$$u_z(x,t) \approx \frac{i}{4}\sqrt{\frac{2}{\pi k_0 x}}e^{i(\frac{\omega_0}{c})x}e^{-\alpha x}e^{i\omega_0 t} \quad \text{(Eq. 21)}$$

By multiplying both sides of the equation by $\sqrt{x}$, and observing that $A=\frac{i}{4}\sqrt{\frac{2}{\pi k_0}}$ is a constant, one obtains

$$(\sqrt{x})u_z(x,t)=Ae^{i(\frac{\omega_0}{c})x}e^{-\alpha x}e^{i\omega_0 t} \quad \text{(Eq. 22)}$$

By comparing the right hand sides of equations (2) and (22), one can note that the two differ in the amplitude of the wave only, and that the relationship between the attenuation (α) and *FWHM* in equation (18) holds for the case of a cylindrical wave field multiplied by the square root of propagation distance vector.

Finite Element Analysis

Finite element analysis simulations were carried out in ABAQUS (version 6.12-1, 3DS Inc., Waltham, MA). The numerical phantom was simulated by a 2D 50 mm × 50 mm planar model of an infinite viscoelastic medium with the density of 1000 kg/m^3 and mechanical properties defined in terms of the Voigt model where the elasticity (μ_1) and viscosity (μ_2) were $\mu_1 = 4$ *kPa* and $\mu_2 = 4$ $Pa \cdot s$, respectively. The harmonic and impulsive excitations (displacement) were applied on one side of the phantom, while the other side was attached to an infinite region to minimize the reflections. The plane waves were excited by vibrating the entire side of the phantom for four full cycles of vibrations. The impulsive waves were excited by moving a single vertical line. The impulse was generated using a raised sine wave with the length of 200 μs. The phantom was meshed with linear quadrilateral elements (type CPE4H) of size 0.25 mm × 0.25 mm. The infinite region was meshed by infinite elements (type CINPE4). The temporal sampling rate was 10 kHz. The finite element model was solved by an implicit dynamic solver with automatic step size control. Mesh convergence tests were performed so that further refining the mesh did not change the solution

significantly. Particle velocity was extracted along the center line of the phantom to minimize the influence of boundary effects.

Polyvinyl Alcohol and Porcine Liver Studies

The polyvinyl alcohol (PVA) phantom was made from a mixture of 10% PVA by weight concentration dissolved in water as described in (Fromageau *et al.*, 2007). Following the heating process, the mixture was poured into a Plexiglas mold with dimensions 8 × 8 × 8 cm. The mixture was allowed to cool to the room temperature and placed in a freezer overnight. The measurements were made the next day. The excised liver was obtained from a local butcher shop the day before the study and was frozen overnight. A programmable ultrasound imaging platform (Verasonics, Inc., Kirkland, WA, USA) operating a 128 element linear array L7-4 transducer with the center frequency of 5 MHz (Philips Healthcare, Andover, MA) was used to excite 400 μs impulse in the PVA and liver phantoms. A mechanical shaker (V203, Ling Dynamic Systems Limited, Hertfordshire, UK) was used to excite plate and cylindrical harmonic waves. A glass rod coupled with the shaker was glued to the material in a hole bored through the thickness of the samples. An acrylic plate 72 mm in width and 96 mm in height was placed on the side of the phantoms and coupled to the shaker to excite plane waves. Four cycles of sinusoidal waves were used to drive the shaker at different frequencies in the range 100–500 Hz. The displacements were on the order of tens of microns. Plane wave imaging detection pulses transmitted at a pulse repetition frequency of 10 kHz with a three angle compounding for an effective frame rate of 3.33 kHz was used to track the motion along the line of propagation (Montaldo *et al.*, 2009). Autocorrelation was used to obtain the displacement field (Loupas *et al.*, 1995).

Patient Studies

The human studies were conducted according to a protocol approved by the Mayo Clinic Institutional Review Board (IRB#15-003367) during previously indicated biopsy studies. Fifteen patients with a liver transplant with a risk of acute cellular rejection who were undergoing clinically-indicated percutaneous liver biopsy were recruited for the study. Liver biopsies were obtained in a standard fashion via percutaneous approach with a core sampling needle on day 7 following the transplant surgery. All biopsy specimens were reviewed by expert pathologists familiar with the interpretation of liver allograft biopsies. Biopsy specimens were permanently fixed and stained with hematoxylin and eosin. The diagnosis of acute cellular rejection was made based on standard histologic criteria which include the presence or absence of portal tract lymphocytic infiltration, bile duct inflammation and venous endothelial inflammation (Demetris *et al.*, 2000). The biopsy studies were compared to the AMUSE measurements of shear wave velocity and attenuation. The subject was laid supine on the examination bed with right arm abducted. For each measurement, a sonographer positioned the transducer using B-mode imaging to locate a relatively large liver region free of major vessels through an intercostal space. Then the subject was instructed to suspend breathing while the operator pressed the button to generate shear waves using ultrasound radiation force and record shear wave motion using high frame rate plane wave imaging technique. For each subject, 30 measurements were obtained at three different focal depths (35, 40, and 45 mm) with 10 repetitions at each focal depth. Each measurement consisted of a leftward and a rightward propagating wave for a

total of 60 measurements. A programmable ultrasound imaging platform (Verasonics, Inc. Kirkland, WA, USA) operating a C5-2 transducer with the center frequency of 3 MHz (Philips Healthcare, Andover, MA) was used to excite shear waves and track the motion. Three angle compounding plane wave imaging detection pulses transmitted at a pulse repetition frequency of 2.78 kHz was used to track the motion (Montaldo *et al.*, 2009).

Results

Figure 1 summarizes the comparison between the traditional methods of calculating the shear wave velocity and attenuation using the phase gradient and amplitude decay, and the novel AMUSE approach. We consider the phase gradient and amplitude decay as laboratory reference methods that were used for comparison with AMUSE measurements. The phase gradient method measures the change of phase as a function of distance $\Delta\varphi/\Delta r$ at a given frequency (f) and calculates the velocity as $c = 2\pi f\Delta r/\Delta\varphi$. The amplitude decay method fits a decaying exponential function (last term in Eq. (3)) to the decaying amplitude of the wave as a function of distance to obtain the attenuation, α. The amplitude decay technique is difficult to perform *in vivo* as it requires very good signal-to-noise ratio (SNR) and the data is typically very noisy. A finite element model (FEM) was used to study shear wave propagation. Plane harmonic, plane impulsive, cylindrical harmonic and cylindrical impulsive excitations were used to propagate waves in the medium. The plane waves were excited by vibrating a plane of elements inside the medium, perpendicular to the direction of wave propagation, which results in a uniform 'planar' wave front. The cylindrical waves were excited by vibrating a single line of elements perpendicular to the direction of wave propagation, resulting in a wave front that cylindrically radiates from the line of excitation. Using a line source is meant to mimic the use of a focused ultrasound beam to create the shear wave with acoustic radiation force. In the case of harmonic plane waves, the shear wave velocities and attenuations obtained using the traditional methods of phase gradient and amplitude decay (Figs. 1(a)–(c)) and the values obtained using AMUSE (Figs. 1(d)–(f)) are close to the theoretical values. Because the impulse contains multiple frequencies, the AMUSE method can extract the shear wave velocity and attenuation at several frequencies by finding the k-space peak at the given frequency, using $c = f/k_x$, formula for the velocity and $\alpha = \frac{FWHM \times \pi}{\sqrt{3}}$ for the attenuation. The sample impulse based measurements at 200 Hz are shown in Fig. 1(i).

Figure 2 shows the differences in the shape of the wave front for the plane harmonic, cylindrical harmonic and cylindrical impulse excitation. Note that the wave fronts for the cylindrical harmonic and impulse excitation have similar shape of the wave front (Figs. 2(e–f)). The wave front due to focused acoustic radiation force is similar to the cylindrical impulse excitation.

Figures 3 and 4 summarize the importance of using the correction factor when estimating the shear wave velocity and attenuation in a cylindrical shear wave. The results in Figs. 3 and 4 validate the shear wave velocity and attenuation measurements obtained using AMUSE against laboratory gold standard measurements. The shear wave velocity measurements were in good agreement with the phase gradient results for all excitation scenarios, while the evaluation of shear wave attenuation due to cylindrical excitation

requires the correction factor. The results in Figs. 3 and 4 validate the AMUSE method from the numeral and experimental perspective.

Following the validation in phantoms, AMUSE was used to measure shear wave velocity and attenuation in 15 liver allografts post-transplant. The results were compared to the biopsy findings as shown in Fig. 5. The average shear wave velocity and attenuation are shown in Fig. 6. The shear wave velocity and attenuation were extracted from the impulsive data at 100, 200, and 300 Hz. At all three frequencies, livers with acute rejection had higher velocity and lower attenuation than livers without acute rejection. We hypothesized that the increase in inflammatory cells present in the setting of acute cellular rejection would change the viscoelastic material properties of the liver and could be used to separate patients with and without acute rejection. The subjects with high attenuation and low velocity corresponded to the clinical findings of livers with no acute rejection. To assess the value of AMUSE results for separating the two groups to obtain a reliable diagnosis, we conducted a statistical analysis based on the Hotelling trace criterion (Fiete *et al.*, 1987). The Hotelling trace criterion measures the goodness of clustering and separation of groups and was used to evaluate the ability of AMUSE to separate the patients with acute rejection versus no acute rejection liver transplants based on the velocity, attenuation, and velocity and attenuation combined. The results are summarized in Fig. 6 and Table I. The Hotelling trace criterion indicating the ability of parameters to separate two groups was better for the shear wave attenuation than velocity at 100 and 200 Hz. Using both the shear wave velocity and attenuation showed better separation power. The results at 300 Hz showed less separation. The results in Table I show that using wave attenuation in addition to the velocity improves the ability to separate the two groups of patients.

The Hotelling trace criterion was used to quantify the ability of the two metrics (velocity and attenuation) to separate the patient cohort into two groups, one with and one without acute cellular rejection. The Hotelling trace criterion measures the goodness of clustering of the data points and the power of separation of the two groups. The Hotelling trace criterion for the velocity($\boldsymbol{c}$), attenuation ($\boldsymbol{\alpha}$) and the combination of the velocity and attenuation ($\boldsymbol{c, \alpha}$)at 100, 200 and 300 Hz are shown in Table I.

Discussion

We demonstrated the theoretical basis for recovering shear wave velocity and attenuation from a harmonic plane wave. Additionally, we showed that the k-space approach can be used in case of the cylindrical wave propagation, which is closer to the wave front due to focused acoustic radiation force. Results in Figs. 3 and 4 show validation of the AMUSE technique in an FEM simulation, a PVA tissue mimicking phantom and an excised pig liver, by comparing them to either the theory and/or our gold standard measurements. The results in Fig. 4 demonstrate the importance of using the $\sqrt{x}$ correction factor in order to obtain the accurate estimates of shear wave attenuation. The correction factor is used to account for the presence of a cylindrical wave when estimating the shear wave attenuation and is applied to the motion data before the Fourier transform. The correction factor was used because there was no obvious closed form analytical solution for cylindrical wave equation. In theory, the correction factor does not influence the shear wave velocity estimates (Eqs. 20–22).

However, the application of the correction factor also assumes presence of a perfectly cylindrical wave, which is beyond one's control in experimental settings. Due to numerical errors, the correction factor could also result in a slight shift of the maxima in k-space, the contribution of which is beyond the scope of this study.

The patient study in Fig. 6 and the results in Table I show that the AMUSE method has the potential to differentiate between the livers with and without acute cellular rejection. Further studies with more subjects are necessary to draw more definite conclusions. In a similar study, Yoon, *et al.* used shear wave elastography to evaluate the presence of ACR in post-transplant livers (Yoon *et al.*, 2013). The Young's moduli for patients with and without ACR were 12.14 ± 5.49 kPa and 6.33 ± 2.10 kPa, respectively. The Young's modulus (E) was calculated via $E = 3\rho c_s^2$, where ρ is the tissue density and c_s is the shear wave velocity. For comparison, the mean shear wave velocities for livers with and without ACR are roughly 2.01 m/s and 1.45 m/s, respectively. These values are similar to our findings in Fig. 6. Studies showing the application of transient elastography ultrasound for monitoring of liver transplants have also been reported (Berenguer and Schuppan, 2013; Cholongitas *et al.*, 2010; Adebajo *et al.*, 2012).

AMUSE was used to measure shear wave velocity and attenuation in 15 transplanted livers, and the results were compared to the biopsy results. The subjects with high attenuation and low velocity corresponded to the clinical findings of livers with no acute rejection, and the subjects with high velocity and low attenuation corresponded to mild acute rejection. The subjects with high velocity and low attenuation corresponded to clinical findings of minimal or mild acute rejection. An explanation for these results may be that the increased cellular infiltration in the livers undergoing acute rejection could cause the shear waves to propagate faster because the cells are packed tighter together in a confined volume and the effective tissue stiffness increases. Additionally, the attenuation decreases because the presence of additional cells in the liver displaces some of the interstitial fluid that may contribute to shear wave attenuation. Accurate estimation of shear wave velocity and attenuation could provide unique diagnostic indicators when combined as demonstrated in the liver transplant example. AMUSE could provide new information for a wide variety of ultrasound and MR-based elastography methods. AMUSE can be used across ultrasound and magnetic resonance shear wave elastography techniques to study other disorders that result in changes of tissue mechanical properties.

Robust measurement of both shear wave velocity and attenuation with the AMUSE method allows for characterization of the viscoelastic properties of soft tissues without fitting data to a rheological model within the viscoelastic medium assumed in Eq. (1). AMUSE results could assist in diagnosis of rejection in liver transplant allografts. AMUSE could be extended to other organs and tissues that could be affected by inflammation and fibrosis as well as to study tissue edema.

It is important to note that the AMUSE method is developed with the assumption of 2D shear wave tracking obtained by the majority of ultrasound probes. The inherent assumption of this technique is the ability to track the wave propagation in-plane. Out-of-plane wave propagation would misestimate the values of shear wave velocity and attenuation. In

addition, due to the necessity for the correction factor to account of the presence of a cylindrical wave, accurate measurements with AMUSE require knowing the origin of the shear wave in space and time. In case of a plane wave, this limitation would not be needed.

The AMUSE method described in this paper was specifically predicated on the assumption of a linear, isotropic, homogeneous, and viscoelastic medium. Many elastographic methods have sought to characterize soft tissues using different sets of parameters despite the incredible complexity of the mechanical behavior of soft tissues. Using a minimal set of parameters to describe the mechanical behavior observed is often desired. For viscoelastic characterization the phase velocity dispersion or measured motion are often fit to models based on a rheological model (Chen *et al.*, 2009; Deffieux *et al.*, 2009; Gennisson *et al.*, 2014). The ultimate aim of this parameterization is to relate simple mechanical elements to the structure of the tissue and understand the measured mechanical behavior, i.e., wave velocity, wave attenuation. However, this type of parameterization requires a number of assumptions to be made that may or may not be valid. In the end, there is a trade-off between using a model with its accompanying assumptions and yielding a parameterization that provides clinically diagnostic elements which separate normal tissue from abnormal tissue. The AMUSE method is an approach to more robustly measure wave attenuation along with phase velocity, which in the case presented in this report on liver transplant characterization provided useful information to separate patients with acute cellular rejection from those without this condition.

Another limitation is the assumption of a cylindrical wave that is created by the acoustic radiation force push. The effects of this assumption were analyzed by Rouze, *et al.*, and how accurate estimation of the attenuation may be affected by the shaped of the acoustic radiation force push beam (Rouze *et al.*, 2015). The AMUSE method is also dependent on other general limitations of ultrasound-based shear wave elastography methods that rely on acoustic radiation force to generate the shear waves. The AMUSE method requires robust wave generation with the acoustic radiation force beam and motion detection methods to track waves that could be affected by phase aberration and attenuation (Amador *et al.*, 2016; Carrascal *et al.*, 2016).

Conclusion

Changes in mechanical properties of soft tissues are related to numerous diseases. The field of shear wave elastography has offered various techniques to measure mechanical properties of biological tissues. All biological tissues are inherently viscoelastic and ignoring the viscous component biases estimates of elasticity and fails to report an important tissue parameter. Measurement of tissue viscoelasticity without a rheological model requires independent measurements of both shear wave velocity and attenuation. We present such a method and refer to it as Attenuation Measuring Ultrasound Shearwave Elastography (AMUSE). AMUSE was used to measure shear wave velocity and attenuation in 15 transplanted livers being assessed for acute rejection. The results show that the shear wave velocity and attenuation can be used to separate the livers with and without acute cellular rejection, and that using both parameters increases the Hotelling trace criterion for separation of groups. The results suggest that AMUSE can be used to assist in diagnosis of

rejection in liver transplants, and can be extended to other organs and tissues that could be affected by inflammation and fibrosis.

Acknowledgments

This work was supported by grants R01EB002167, R01DK082408, and R01DK092255 from the National Institute of Biomedical Imaging and Bioengineering (NIBIB), the National Institute of Diabetes and Digestive and Kidney Disease (NIDDK), the National Institutes of Health (NIH). The content is solely the responsibility of the authors and does not necessarily represent the official views of the NIBIB, NIDDK, and NIH. This research was also supported by the Mayo Clinic Center for Individualized Medicine Imaging Biomarker Grant. The authors would like to thank Duane Meixner for performing ultrasound scans.

References

Achenbach, JD. Amsterdam, The Netherlands: Elsevier Science Publishers B. V; 2005. p. 10-165.

Adebajo CO, Talwalkar JA, Poterucha JJ, Kim WR, Charlton MR. Ultrasound-based transient elastography for the detection of hepatic fibrosis in patients with recurrent hepatitis C virus after liver transplantation: a systematic review and meta-analysis. Liver Transpl. 2012; 18:323–31. [PubMed: 22140010]

Amador C, Song P, Meixner DD, Chen S, Urban MW. Improvement of Shear Wave Motion Detection Using Harmonic Imaging in Healthy Human Liver. 2016; 42:1031–41.

Asbach P, Klatt D, Hamhaber U, Braun J, Somasundaram R, Hamm B, Sack I. Assessment of liver viscoelasticity using multifrequency MR elastography. Magn Reson Med. 2008; 60:373–9. [PubMed: 18666132]

Asbach P, Klatt D, Schlosser B, Biermer M, Muche M, Rieger A, Loddenkemper C, Somasundaram R, Berg T, Hamm B, Braun J, Sack I. Viscoelasticity-based staging of hepatic fibrosis with multifrequency MR elastography. Radiology. 2010; 257:80–6. [PubMed: 20679447]

Bercoff J, Tanter M, Fink M. Supersonic shear imaging: a new technique for soft tissue elasticity mapping. IEEE transactions on ultrasonics, ferroelectrics, and frequency control. 2004; 51:396–409.

Berenguer M, Schuppan D. Progression of liver fibrosis in post-transplant hepatitis C: mechanisms, assessment and treatment. J Hepatol. 2013; 58:1028–41. [PubMed: 23262248]

Bernal M, Nenadic I, Urban MW, Greenleaf JF. Material property estimation for tubes and arteries using ultrasound radiation force and analysis of propagating modes. The Journal of the Acoustical Society of America. 2011; 129:1344–54. [PubMed: 21428498]

Carrascal CA, Aristizabal S, Greenleaf JF, Urban MW. Phase Aberration and Attenuation Effects on Acoustic Radiation Force-Based Shear Wave Generation. 2016; 63:222–32.

Chen S, Sanchez W, Callstrom MR, Gorman B, Lewis JT, Sanderson SO, Greenleaf JF, Xie H, Shi Y, Pashley M, Shamdasani V, Lachman M, Metz S. Assessment of liver viscoelasticity by using shear waves induced by ultrasound radiation force. Radiology. 2013; 266:964–70. [PubMed: 23220900]

Chen S, Urban MW, Pislaru C, Kinnick R, Zheng Y, Yao A, Greenleaf JF. Shearwave dispersion ultrasound vibrometry (SDUV) for measuring tissue elasticity and viscosity. IEEE transactions on ultrasonics, ferroelectrics, and frequency control. 2009; 56:55–62.

Cholongitas E, Tsochatzis E, Goulis J, Burroughs AK. Noninvasive tests for evaluation of fibrosis in HCV recurrence after liver transplantation: a systematic review. Transpl Int. 2010; 23:861–70. [PubMed: 20704691]

Company T N Y T. NYT Liver Biopsy Image. 2007

Couade M, Pernot M, Messas E, Bel A, Ba M, Hagege A, Fink M, Tanter M. In vivo quantitative mapping of myocardial stiffening and transmural anisotropy during the cardiac cycle. IEEE transactions on medical imaging. 2011; 30:295–305. [PubMed: 20851788]

Couade M, Pernot M, Prada C, Messas E, Emmerich J, Bruneval P, Criton A, Fink M, Tanter M. Quantitative assessment of arterial wall biomechanical properties using shear wave imaging. Ultrasound in medicine & biology. 2010; 36:1662–76. [PubMed: 20800942]

Deffieux T, Montaldo G, Tanter M, Fink M. Shear wave spectroscopy for in vivo quantification of human soft tissues visco-elasticity. IEEE transactions on medical imaging. 2009; 28:313–22. [PubMed: 19244004]

Demetris A, Adams D, Bellamy C, Blakolmer K, Clouston A, Dhillon AP, Fung J, Gouw A, Gustafsson B, Haga H, Harrison D, Hart J, Hubscher S, Jaffe R, Khettry U, Lassman C, Lewin K, Martinez O, Nakazawa Y, Neil D, Pappo O, Parizhskaya M, Randhawa P, Rasoul-Rockenschaub S, Reinholt F, Reynes M, Robert M, Tsamandas A, Wanless I, Wiesner R, Wernerson A, Wrba F, Wyatt J, Yamabe H. Update of the International Banff Schema for Liver Allograft Rejection: working recommendations for the histopathologic staging and reporting of chronic rejection. An International Panel. Hepatology. 2000; 31:792–9. [PubMed: 10706577]

Fiete RD, Barrett HH, Smith WE, Myers KJ. Hotelling trace criterion and its correlation with human-observer performance. J Opt Soc Am A. 1987; 4:945–53. [PubMed: 3598746]

Fromageau J, Gennisson JL, Schmitt C, Maurice RL, Mongrain R, Cloutier G. Estimation of polyvinyl alcohol cryogel mechanical properties with four ultrasound elastography methods and comparison with gold standard testings. IEEE transactions on ultrasonics, ferroelectrics, and frequency control. 2007; 54:498–509.

Gennisson JL, Deffieux T, Mace E, Montaldo G, Fink M, Tanter M. Viscoelastic and anisotropic mechanical properties of in vivo muscle tissue assessed by supersonic shear imaging. Ultrasound in medicine & biology. 2010; 36:789–801. [PubMed: 20420970]

Gennisson JL, Marcellan A, Dizeux A, Tanter M. Rheology over five orders of magnitude in model hydrogels: agreement between strain-controlled rheometry, transient elastography, and supersonic shear wave imaging. IEEE transactions on ultrasonics, ferroelectrics, and frequency control. 2014; 61:946–54.

Graff, KF. London, UK: Oxford University Press; 1975. p. 273-310.

Klatt D, Friedrich C, Korth Y, Vogt R, Braun J, Sack I. Viscoelastic properties of liver measured by oscillatory rheometry and multifrequency magnetic resonance elastography. Biorheology. 2010; 47:133–41. [PubMed: 20683156]

Kundu, T. New York: CRC Press; 2003. p. 1-95.

Leclerc GE, Charleux F, Robert L, Ho Ba Tho MC, Rhein C, Latrive JP, Bensamoun SF. Analysis of liver viscosity behavior as a function of multifrequency magnetic resonance elastography (MMRE) postprocessing. J Magn Reson Imaging. 2013; 38:422–8. [PubMed: 23293060]

Loupas T, Peterson RB, Gill RW. Experimental evaluation of velocity and power estimation for ultrasound blood flow imaging, by means of a two-dimensional autocorrelation approach. 1995; 42:689–99.

Montaldo G, Tanter M, Bercoff J, Benech N, Fink M. Coherent plane-wave compounding for very high frame rate ultrasonography and transient elastography. IEEE transactions on ultrasonics, ferroelectrics, and frequency control. 2009; 56:489–506.

Muller M, Gennisson JL, Deffieux T, Tanter M, Fink M. Quantitative viscoelasticity mapping of human liver using supersonic shear imaging: preliminary in vivo feasibility study. Ultrasound in medicine & biology. 2009; 35:219–29. [PubMed: 19081665]

Nenadic IZ, Urban MW, Mitchell SA, Greenleaf JF. Lamb wave dispersion ultrasound vibrometry (LDUV) method for quantifying mechanical properties of viscoelastic solids. Physics in medicine and biology. 2011; 56:2245–64. [PubMed: 21403186]

Nightingale KR, Rouze NC, Rosenzweig SJ, Wang MH, Abdelmalek MF, Guy CD, Palmeri ML. Derivation and analysis of viscoelastic properties in human liver: impact of frequency on fibrosis and steatosis staging. IEEE transactions on ultrasonics, ferroelectrics, and frequency control. 2015; 62:165–75.

Rouze NC, Palmeri ML, Nightingale KR. An analytic, Fourier domain description of shear wave propagation in a viscoelastic medium using asymmetric Gaussian sources. 2015; 138:1012–22.

Sarvazyan A, Hall TJ, Urban MW, Fatemi M, Aglyamov SR, Garra BS. An Overview of Elastography - an Emerging Branch of Medical Imaging. Curr Med Imaging Rev. 2011; 7:255–82. [PubMed: 22308105]

Sebag F, Vaillant-Lombard J, Berbis J, Griset V, Henry JF, Petit P, Oliver C. Shear wave elastography: a new ultrasound imaging mode for the differential diagnosis of benign and malignant thyroid nodules. J Clin Endocrinol Metab. 2010; 95:5281–8. [PubMed: 20881263]

Sinkus R, Tanter M, Catheline S, Lorenzen J, Kuhl C, Sondermann E, Fink M. Imaging anisotropic and viscous properties of breast tissue by magnetic resonance-elastography. Magn Reson Med. 2005; 53:372–87. [PubMed: 15678538]

Tanter M, Bercoff J, Athanasiou A, Deffieux T, Gennisson JL, Montaldo G, Muller M, Tardivon A, Fink M. Quantitative assessment of breast lesion viscoelasticity: initial clinical results using supersonic shear imaging. Ultrasound in medicine & biology. 2008; 34:1373–86. [PubMed: 18395961]

Tanter M, Fink M. Ultrafast imaging in biomedical ultrasound. IEEE transactions on ultrasonics, ferroelectrics, and frequency control. 2014; 61:102–19.

Yoon JH, Lee JY, Woo HS, Yu MH, Lee ES, Joo I, Lee KB, Yi NJ, Lee YJ, Han JK, Choi BI. Shear wave elastography in the evaluation of rejection or recurrent hepatitis after liver transplantation. Eur Radiol. 2013; 23:1729–37. [PubMed: 23300037]

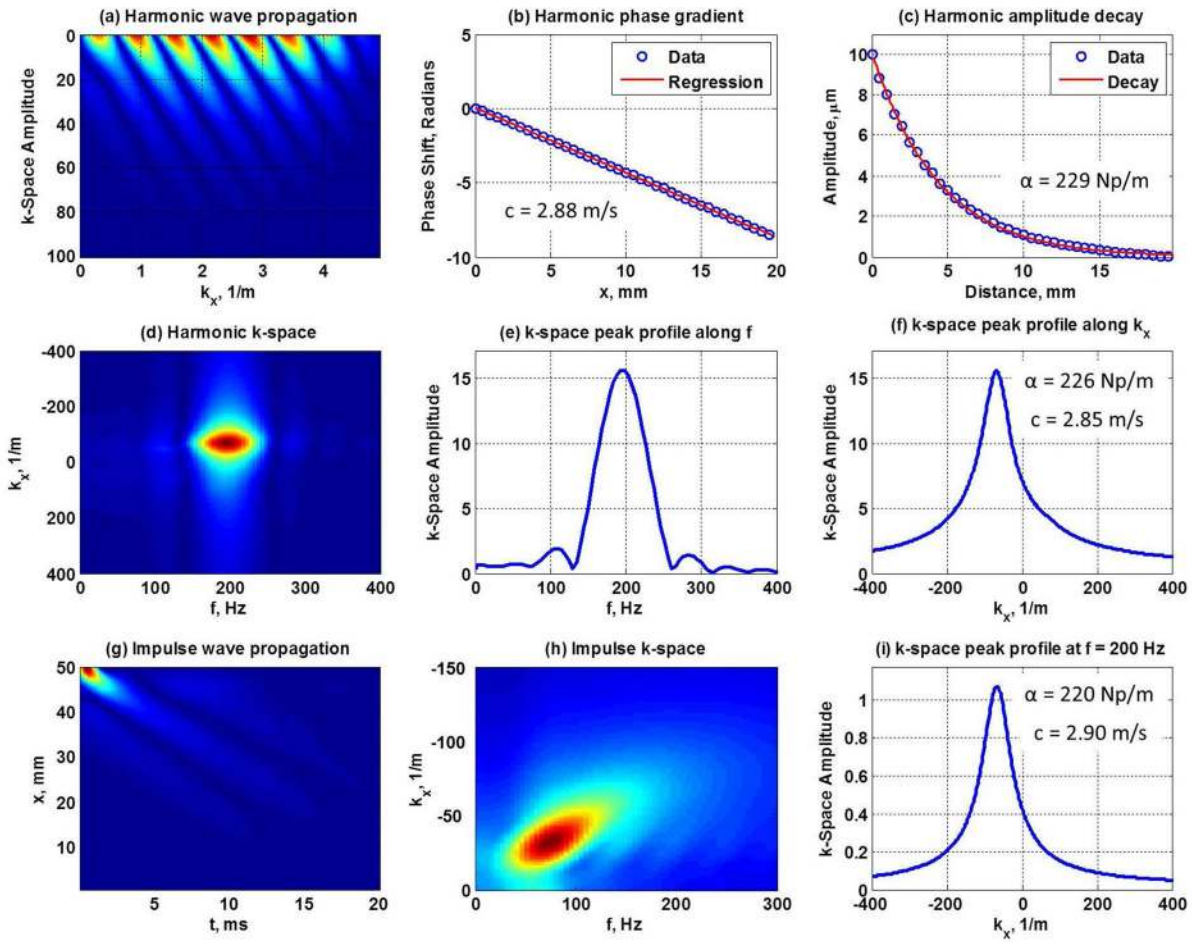

Figure 1.

Finite element model (FEM) analysis was used to model shear wave propagation in a viscoelastic medium at 200 Hz. The wave propagation as a function of time and distance (a) was used to calculate the shear wave velocity and attenuation using the gold standard methods of phase gradient (b) and amplitude decay (c) (values shown). A new method is based on performing a 2D FT of the wave propagation shown in (a) to obtain the k-space shown in (d), with the energy peak in at 200 Hz. The coordinates of the k-space are the frequency (f) and wave number (k_x). The profiles of the peak along the frequency axis is shown in (e) and along the wave number axis in (f). Because the velocity $\boldsymbol{c = f/k_x}$, the wave velocity can be calculated directly from the k-space by finding the peak at the given frequency and dividing the f–coordinate by the k_x– coordinate. The shear wave attenuation can be calculated by measuring the full-width-at-half-maximum ($FWHM$) of the peak in (f) and formula $\alpha = \frac{FWHM \times \pi}{\sqrt{3}}$ (values shown). In case of an impulsive wave which contains multiple frequencies (g), the 2D FFT (h) has peaks at several frequencies. The shear wave velocity and attenuation at each frequency can be obtained by taking the profile along the k_x–axis at each frequency. Panel (i) shows a sample calculation at 200 Hz (values shown). The true values are $c = 2.85$ m/s and $\alpha = 219$ Np/m ($\mu_1 = 4$ kPa and $\mu_2 = 4$ Pa·s, and the Voigt relationship, $2\pi f_0/c + i\alpha = 2\pi f_0 ((\mu_1 + i2\pi f_0\mu_2)/\rho)^{-1/2}$, is evaluated at $f_0 = 200$ Hz).

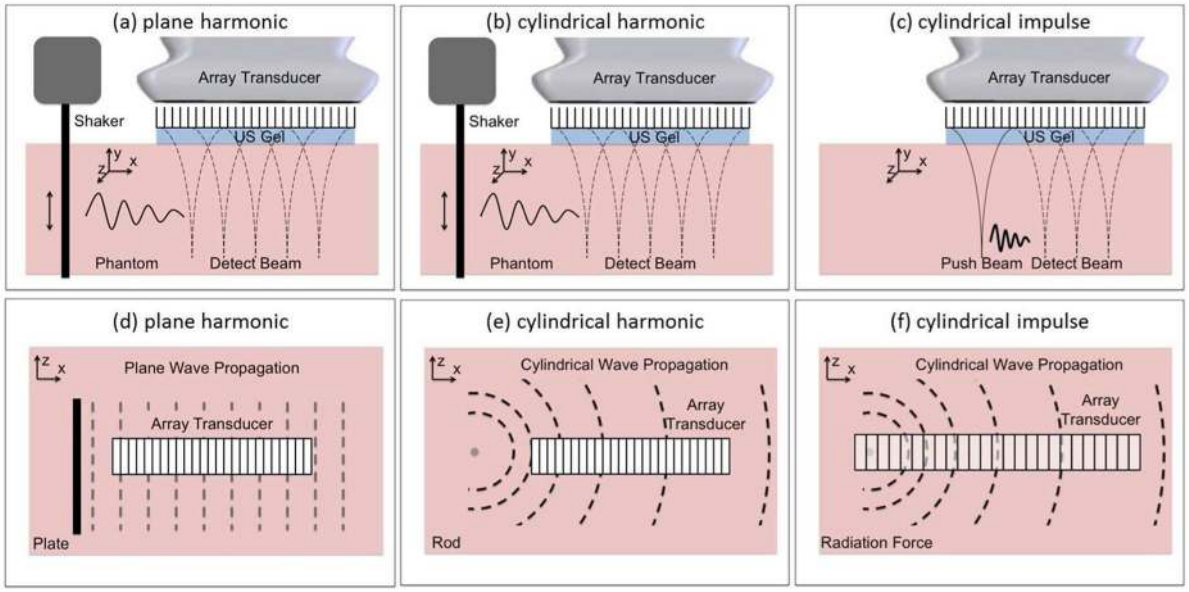

Figure 2.

Shear wave velocity is the rate of wave energy propagation as a function of time and distance, while the shear wave attenuation is the rate of wave energy dissipation as a function of distance. The shear wave velocity is unaffected by the shape of the wave front and the plane harmonic, cylindrical harmonic and cylindrical impulse excitations ((a)–(c)) result in the same shear wave velocity at a given frequency. The shear wave attenuation estimate, however, does depend on the nature of excitation since attenuation depends on the shape of the wave front of energy dissipation ((d)–(f)). Appropriate correction factors must be considered to correct for the cylindrical and spherical wave propagation. Shear wave ultrasound vibrometry methods use focused radiation force to move tissue and the geometry of such excitation can be approximated by a cylindrical source.

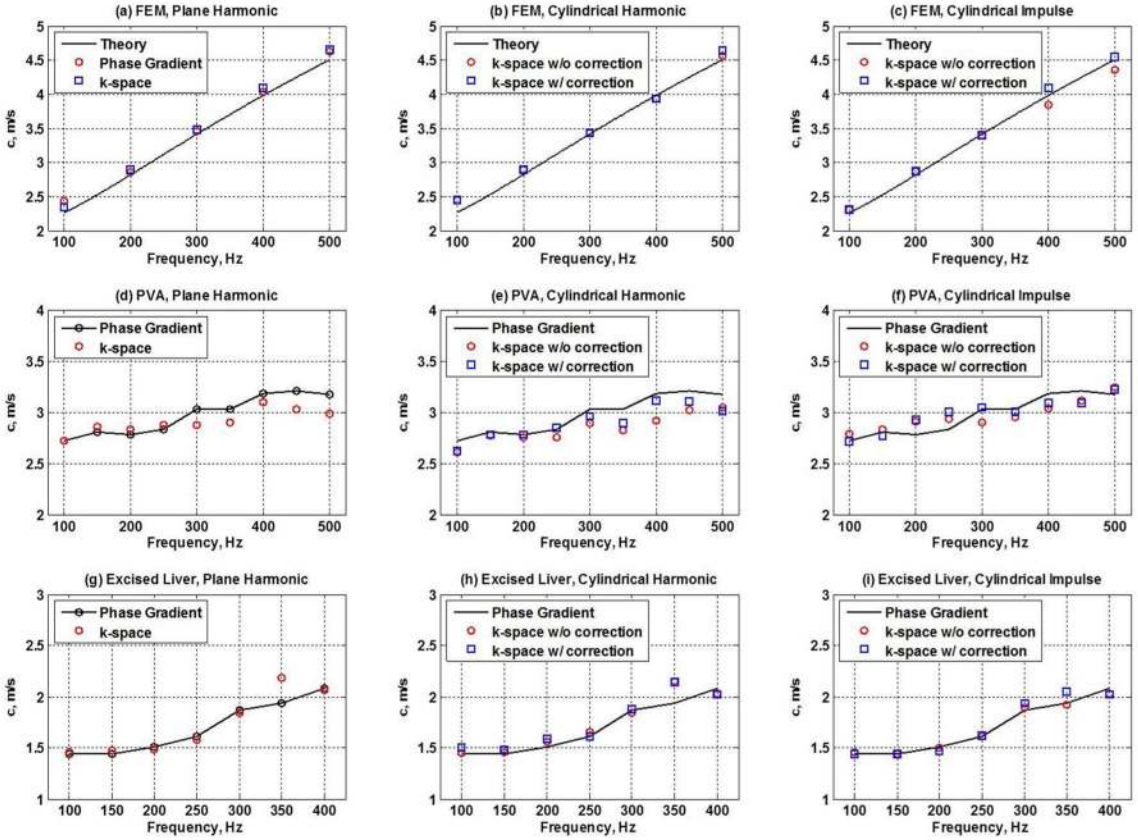

Figure 3.

Shear wave velocity was measured in the FEM simulation, PVA phantom and excised pig liver. In each medium, plane harmonic, cylindrical harmonic and cylindrical impulse sources were used to excite shear waves. In the FEM, the theoretical prediction curve is plotted as a solid line for comparison. In case of the PVA and excised liver phantoms, the velocity estimates using the phase gradient were considered the gold stand and are plotted for comparison. In the FEM, the velocity calculations using the phase gradient and the k-space method in plane harmonic waves are in good agreement with the theoretical curve (a); the k-space-based velocities with and without the $\sqrt{x}$ correction for cylindrical harmonic waves are close to the theoretical values (b); similar pattern is observed in case of cylindrical impulse propagation (c). In the PVA phantom, the phase gradient and the k-space method are in good agreement for the harmonic plane wave propagation (d); the k-space based velocities with and without the correction in case of cylindrical harmonic waves are similar to the plane wave phase gradient measurements (e), as are the k-space velocities due to impulse (f). The pattern is similar in the excised pig liver (g)–(i).

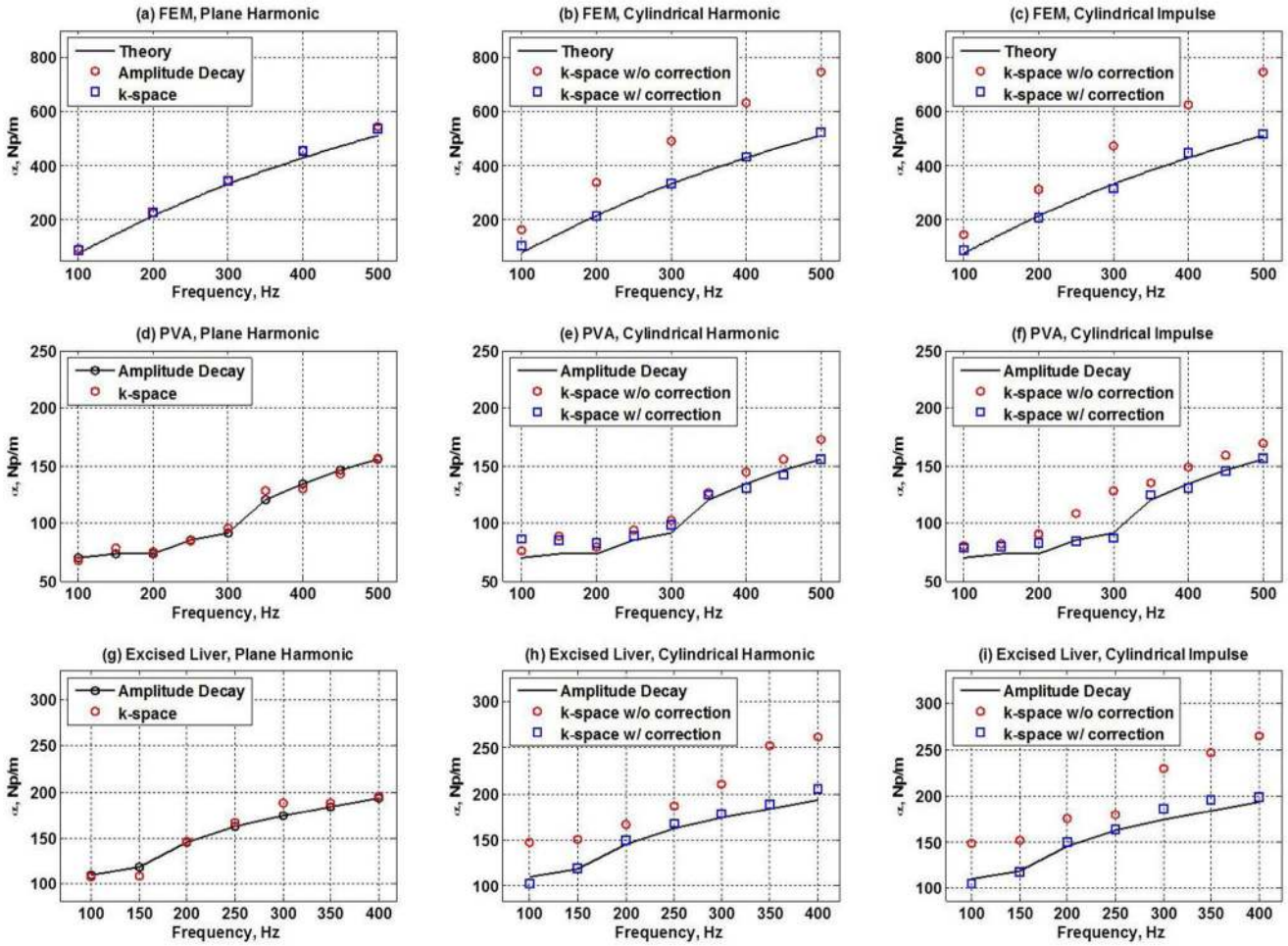

Figure 4.

Shear wave attenuation was measured in the FEM simulation, PVA phantom and excised pig liver. Plane harmonic, cylindrical harmonic and cylindrical impulse sources were used to excite shear waves. In the FEM, the theoretical prediction curve is plotted as a solid line for comparison. In PVA and excised liver, the attenuation estimates using the amplitude decay were considered the gold stand and are plotted for comparison. In the FEM, the attenuations calculated from the amplitude decay and the k-space for plane harmonic waves are in good agreement with the theory (a); the k-space estimates with the $\sqrt{x}$ correction for cylindrical harmonic waves are close to the theoretical values, while the estimates without the correction are not (b); similar pattern is observed for cylindrical impulse propagation (c). In PVA, the amplitude decay and the k-space method are in good agreement for the harmonic plane wave propagation (d); the k-space attenuations with the correction in case of cylindrical harmonic waves are similar to the gold standard values, while the estimates without the correction are not as close (e); this pattern persists in case of the cylindrical impulse (f). The results are similar in the excised pig liver (g)–(i).

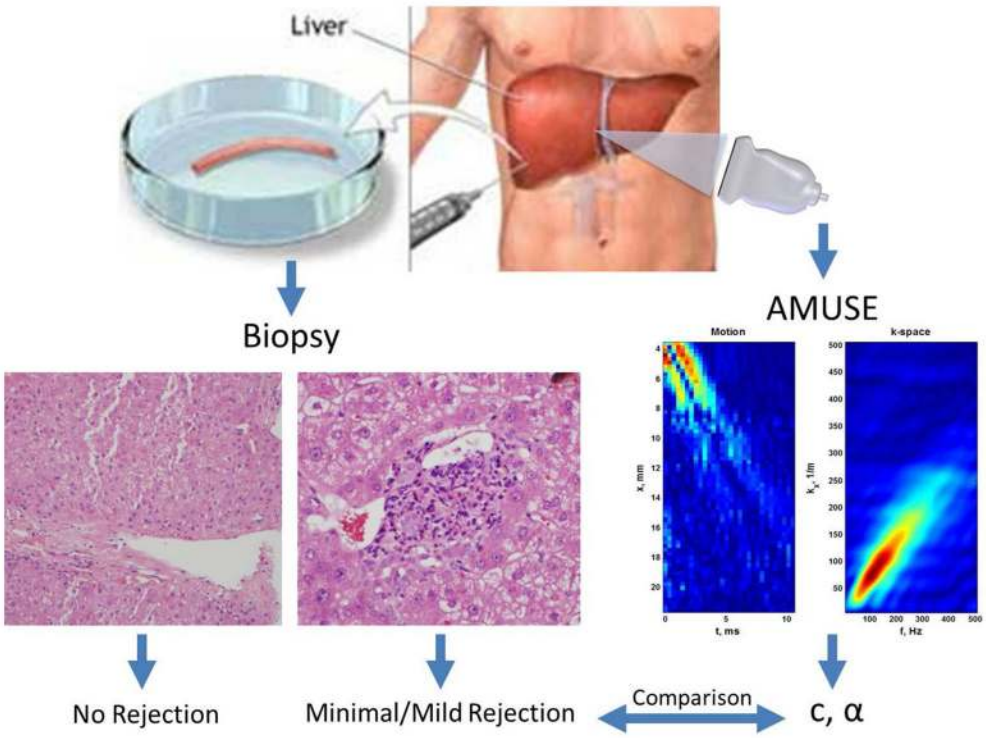

Figure 5.

AMUSE was used to measure shear wave velocity and attenuation in 15 transplanted livers post-transplant. The results were compared to clinical diagnoses made by liver biopsy. The patients were recruited from a cohort of patients undergoing clinical biopsies to assess for potential acute cellular rejection of the transplanted liver. During acute cellular rejection, the number of lymphocytes in the liver increases, while the overall fluid content of the liver remains relatively constant. Histological analysis of acute cellular rejection liver biopsies revealed increase of lymphocytes and plasma cells surrounding the portal tracts, as can be seen in the photomicrographs for the minimal/mild rejection. For each liver, 60 biopsy-like shear wave radiation force-based elastography measurements were made. The AMUSE processing method was used to obtain the shear wave velocity and attenuation at 100, 200 and 300 Hz for all of the subjects. The results are summarized and compared to the biopsy findings in Figure 6 and Table I. (modified from (Company, 2007)).

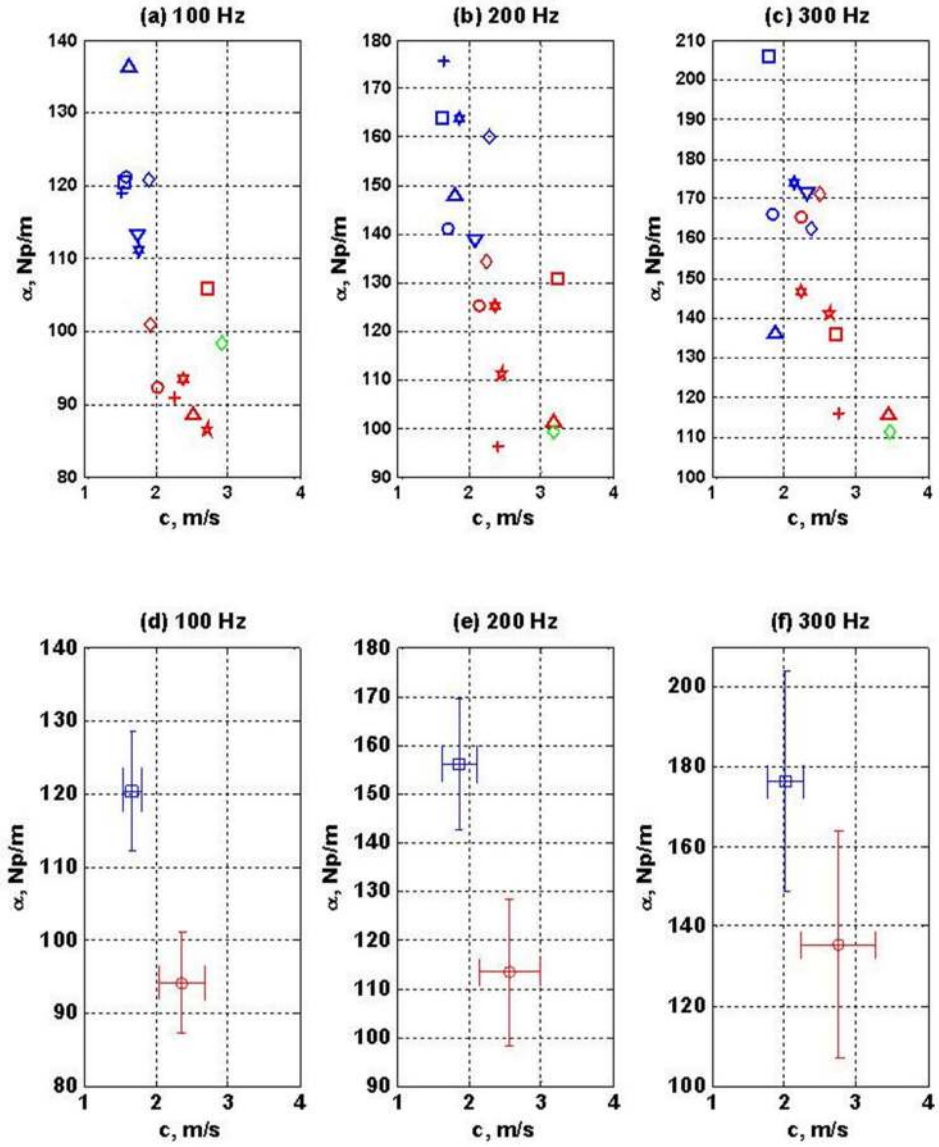

Figure 6.

AMUSE was used to measure shear wave velocity and attenuation in 15 patients' liver allografts following transplantation. Liver biopsy assessed the level of acute cellular rejection in all of the patients. Data points in red correspond to patients with minimal or mild rejection and data points in blue correspond to patients with no rejection. The data points in green correspond to a fibrotic allograft and were not used in further analysis. Panels (a)–(c) show the values of velocity and attenuation for the 15 patients at 100, 200 and 300 Hz. The velocity and attenuation values belonging to each group were separated and the average and standard deviation was computed for both the velocity and attenuation. The results at each frequency are shown in panels (d)–(f).

Table I

Summary of the Hotelling trace criterion for the shear wave velocity, shear wave attenuation and the combination of the two at 100, 200 and 300 Hz.

	100 Hz	200 Hz	300 Hz
c	2.4	1.2	1.0
α	3.6	2.6	0.6
c, α	5.1	2.7	1.1